University of Pennsylvania
ScholarlyCommons

Departmental Papers (BE) | Department of Bioengineering

10-9-2009

Sub-cellular trafficking and functionality of 2'-O-methyl and 2'-O-methyl-phosphorothioate molecular beacons

Anthony K. Chen
University of Pennsylvania, antony@seas.upenn.edu

Mark A. Behlke
Integrated DNA Technologies

Andrew Tsourkas
University of Pennsylvania, atsourk@seas.upenn.edu

Follow this and additional works at: http://repository.upenn.edu/be_papers

Recommended Citation

Chen, A. K., Behlke, M. A., & Tsourkas, A. (2009). Sub-cellular trafficking and functionality of 2'-O-methyl and 2'-O-methyl-phosphorothioate molecular beacons. Retrieved from http://repository.upenn.edu/be_papers/149

The definitive publisher-authenticated version of:
Chen AK, Behlke MA, Tsourkas A. Sub-cellular trafficking and functionality of 2'-O-methyl and 2'-O-methyl-phosphorothioate molecular beacons. Nucleic Acids Res. 2009 Oct 9.
is available online at:
http://nar.oxfordjournals.org/
doi:10.1093/nar/gkp837

This paper is posted at ScholarlyCommons. http://repository.upenn.edu/be_papers/149
For more information, please contact libraryrepository@pobox.upenn.edu.

Sub-cellular trafficking and functionality of 2'-O-methyl and 2'-O-methyl-phosphorothioate molecular beacons

Abstract
Molecular beacons (MBs) have shown great potential for the imaging of RNAs within single living cells; however, the ability to perform accurate measurements of RNA expression can be hampered by false-positives resulting from nonspecific interactions and/or nuclease degradation. These false-positives could potentially be avoided by introducing chemically modified oligonucleotides into the MB design. In this study, fluorescence microscopy experiments were performed to elucidate the subcellular trafficking, false-positive signal generation, and functionality of 2'-O-methyl (2Me) and 2'-O-methyl-phosphorothioate (2MePS) MBs. The 2Me MBs exhibited rapid nuclear sequestration and a gradual increase in fluorescence over time, with nearly 50% of the MBs being opened nonspecifically within 24 h. In contrast, the 2MePS MBs elicited an instantaneous increase in false-positives, corresponding to ~5–10% of the MBs being open, but little increase was observed over the next 24 h. Moreover, trafficking to the nucleus was slower. After 24 h, both MBs were localized in the nucleus and lysosomal compartments, but only the 2MePS MBs were still functional. When the MBs were retained in the cytoplasm, via conjugation to NeutrAvidin, a significant reduction in false-positives and improvement in functionality was observed. Overall, these results have significant implications for the design and applications of MBs for intracellular RNA measurement.

Comments
The definitive publisher-authenticated version of:

Chen AK, Behlke MA, Tsourkas A. Sub-cellular trafficking and functionality of 2'-O-methyl and 2'-O-methyl-phosphorothioate molecular beacons. Nucleic Acids Res. 2009 Oct 9.

is available online at:

http://nar.oxfordjournals.org/
doi:10.1093/nar/gkp837

This journal article is available at ScholarlyCommons: http://repository.upenn.edu/be_papers/149

Nucleic Acids Research Advance Access published October 9, 2009

Nucleic Acids Research, 2009, 1–11
doi:10.1093/nar/gkp837

Sub-cellular trafficking and functionality of 2′-*O*-methyl and 2′-*O*-methyl-phosphorothioate molecular beacons

Antony K. Chen[1], Mark A. Behlke[2] and Andrew Tsourkas[1,*]

[1]Department of Bioengineering, University of Pennsylvania, Philadelphia, PA 19104 and [2]Integrated DNA Technologies, Inc., Coralville, IA 52241, USA

Received June 17, 2009; Revised September 17, 2009; Accepted September 22, 2009

ABSTRACT

Molecular beacons (MBs) have shown great potential for the imaging of RNAs within single living cells; however, the ability to perform accurate measurements of RNA expression can be hampered by false-positives resulting from nonspecific interactions and/or nuclease degradation. These false-positives could potentially be avoided by introducing chemically modified oligonucleotides into the MB design. In this study, fluorescence microscopy experiments were performed to elucidate the subcellular trafficking, false-positive signal generation, and functionality of 2′-*O*-methyl (2Me) and 2′-*O*-methyl-phosphorothioate (2MePS) MBs. The 2Me MBs exhibited rapid nuclear sequestration and a gradual increase in fluorescence over time, with nearly 50% of the MBs being opened nonspecifically within 24 h. In contrast, the 2MePS MBs elicited an instantaneous increase in false-positives, corresponding to ~5–10% of the MBs being open, but little increase was observed over the next 24 h. Moreover, trafficking to the nucleus was slower. After 24 h, both MBs were localized in the nucleus and lysosomal compartments, but only the 2MePS MBs were still functional. When the MBs were retained in the cytoplasm, via conjugation to NeutrAvidin, a significant reduction in false-positives and improvement in functionality was observed. Overall, these results have significant implications for the design and applications of MBs for intracellular RNA measurement.

INTRODUCTION

It has long been recognized that RNAs play an important role in the regulation of cell function and behavior. This has led to the development of numerous techniques capable of measuring gene expression and/or differences in gene expression levels between populations of cells. Commonly used techniques include reverse-transcriptase polymerase chain reaction (RT-PCR), northern blotting and microarrays. Although the value of these population-based measurements cannot be disputed, it has become more and more evident that important information could be overlooked. For example, recent evidence has suggested that genetically identical populations could exhibit large cell-to-cell variations in gene expression and this stochasticity can drive phenotypic diversity and cell fate (1–5). Although methods such a RT-PCR can be adapted to study RNA expression within single cells, due to the complexity of this technique, fluorescence *in situ* hybridization (FISH) generally remains the method of choice for the single cell analysis of RNA expression. Recent advances in FISH have extended the value of this technique by allowing for the visualization of individual RNA and miRNA transcripts within single cells (6–9); however, despite these advances, FISH remains severely limited in its ability to capture the dynamics of gene expression.

In order to obtain a more complete spatial-temporal profile of gene expression, much effort has recently been devoted to developing probes for imaging RNA in single living cells. One promising tool is the molecular beacon (MB), which is an antisense oligonucleotide probe labeled with a 'reporter' fluorophore at one end and a quencher at the other end (10). In the absence of complementary nucleic acid targets, the MBs form a hairpin structure, which brings the fluorophore and quencher into close proximity, creating a low fluorescent state. Hybridization with complementary nucleic acids targets results in the separation of the reporter fluorophore from the quencher and thus fluorescence is restored. The unique ability of MBs to convert target recognition into a detectable fluorescent signal has led to their use in numerous live cell applications, ranging from monitoring the transport and distribution of beta-actin mRNAs in

*To whom correspondence should be addressed. Tel: +1 215 898 8167; Fax: +1 215 573 2071; Email: atsourk@seas.upenn.edu

© The Author(s) 2009. Published by Oxford University Press.
This is an Open Access article distributed under the terms of the Creative Commons Attribution Non-Commercial License (http://creativecommons.org/licenses/by-nc/2.5/uk/) which permits unrestricted non-commercial use, distribution, and reproduction in any medium, provided the original work is properly cited.

motile fibroblasts to detecting the effect of therapeutics on oncogene expression in breast cancer cells (11–29).

Although molecular beacons have clearly shown great promise in the sensitive visualization of RNA in living cells, considerable efforts are now being devoted to optimizing the molecular beacon design to eliminate false-positive signals resulting from nonspecific protein interactions and/or nuclease degradation. For example, we recently found that false-positive signals could simply be avoided by retaining MBs within the cytoplasm, even when nuclease-sensitive DNA backbones are incorporated into the MB design (12,13). Cytoplasmic localization was accomplished through the conjugation of MBs to quantum dots and macromolecules (e.g. NeutrAvidin). Presumably, cytoplasmic localization and the associated elimination of false-positive signals could also be achieved through the coupling of MBs to tRNA. It has previously been shown that tRNA can be used to drive the nuclear export of MBs (15).

As an alternative to retaining MBs in the cytoplasm, it is possible that MBs could also be synthesized with chemically modified oligonucleotide backbones to confer more biostability compared with 2′-deoxy MBs (30,31). To this end, MBs composed of 2′-*O*-methyl- (2Me), locked nucleic acid (LNA)-DNA chimeras, and 2′-*O*-methyl phosphorothioate (2MePS) backbones have been utilized for the long term intracellular monitoring of gene expression (11,15,21,28,29). In one recent study, 2MePS MBs were used to image viral replication in kidney cells for up to 12 h. The results were extremely promising and insightful; however, the subcellular trafficking of the 2MePS MBs and their ability to avoid nonspecific interactions was not systematically evaluated. A better understanding of this behavior is expected to be important in applications where lower copy number RNAs must be detected. Therefore, in this work, we examined the performance of 2MePS MBs in living cells and compared their behavior with 2Me MBs. In addition, we also evaluated how the retention of each MB within the cytoplasm, via conjugation to NeutrAvidin, affected its stability and functionality. Overall, this study provides insights into the fate of molecular beacons in the intracellular environment and is expected to benefit the design of MBs for more accurate and sensitive intracellular measurements of RNA.

MATERIALS AND METHODS

MB design

Antisense firefly luciferase 2Me RNA MBs and 2MePS MBs possessing a TEX 615 fluorophore (Ex: 596 nm, Em: 615 nm) at the 5′-end, an Iowa Black RQ quencher, IBRQ, at the 3′-end and a biotin-dT group incorporated in the 3′ stem was synthesized by Integrated DNA Technologies, Inc. (Coralville, IA, USA). The antisense sequence of firefly luciferase (pGL3-Luc 235-252, Promega, Madison, WI, USA) was chosen because it is not complementary to any known endogenous RNA target in MEF/3T3 cells. Specifically, the antisense 2Me RNA MBs and 2'MePS MBs employed were TEX615-mGmUmCmAmCmCmUmCmAmGmCmGmUmAmAmGmUmGmAmUmGmUmCmG/iBiodT/mGmAmC/3IAbRQSp/and TEX615-mG*mU*mC*mA*mC*mC*mU*mC*mA*mG*mC*mG*mU*mA*mA*mG*mU*mG*m

A*mU*mG*mU*mC*mG*/iBiodT/*mG*mA*mC/3IAbRQSp/, respectively. Luciferase target DNA oligonucleotides were also synthesized, with the sequence: GT CACGACATCACTTACGCTGAGTTT.

Synthesis of fluorescently labeled dextran and NeutrAvidin-MB conjugates

Aminodextran (MW:10k Da, Invitrogen) was dissolved in 50 mM sodium borate buffer (pH 8) at a concentration of 10 mg/ml and reacted with 2.5 mM Alexa750 NHS ester (Invitrogen) at a dye to dextran ratio of 2.5:1. The fluorescently labeled dextrans were purified on NAP-5 gel chromatography columns (Amersham Biosciences) in phosphate buffer (48 mM K_2HPO_4, 4.5 mM KH_2PO_4, 14 mM NaH_2PO_4), pH 7.2. The concentration of the Alexa750 fluorophore was determined spectrophotometrically using a Cary100 spectrophotometer (Varian).

NeutrAvidin (Thermo Scientific) was dissolved in 50 mM sodium borate buffer, pH 8 at a concentration of 10 mg/ml and reacted with 416.7 μM Alexa750-NHS ester (Invitrogen) at dye to NeutrAvidin molar ratio of 2.5:1. The fluorescent conjugates were purified on NAP-5 gel chromatography columns (Amersham Biosciences) in phosphate Buffer, pH 7.2. The number of fluorophores per NeutrAvidin was determined spectrophotometrically. It was determined that here were 1.9 Alexa750 fluorophores per NeutrAvidin. Pegylated NeutrAvidin conjugates was synthesized by further reacting fluorescently labeled NeutrAvidins with Methyl PEOn-NHS ester (10 kDa MW, Laysan) at the 100:1 PEG to NeutrAvidin molar ratio, and purified by repeated filtration and dilution on Microcon YM-50 centrifugal devices (50 000 MW cutoff; Millipore). Initial experiments indicated that when the pegylated NeutrAvidins were microporated into MEF/3T3 cells, the 100:1 PEG labeling ratio yielded a diffuse cytoplasmic distribution of NeutrAvidin as determined by fluorescence microscopy. Microporation and fluorescence microscopy protocols are described below. MB-NeutrAvidin conjugates were synthesized by reacting MBs with purified, fluorescently labeled and pegylated NeutrAvidins at a molar ratio of 1.5:1 MB to NeutrAvidin. All conjugation reactions were allowed to react overnight at room temperature. All conjugates were purified by repeated filtration and dilution on YM-50 centrifugal devices. Concentrations were subsequently determined spectrophotometrically.

Cell culture

MEF/3T3 cells (ATCC, Manassas, VA, USA) were cultured in Dulbeco's MEM media supplemented with 1% Penn/Strep, 10% fetal bovine serum and incubated in 5% CO_2 at 37°C.

Cellular delivery of MB and MB-conjugates

Microinjection. Microinjection of MEF/3T3 cells was performed using a Femtojet and Injectman NI 2 (Eppendorf) microinjection system fitted with Femtotips I (Eppendorf). Prior to use, Femtotips were treated with Hexamethyldisilazne (Fluka) for 10 min, followed by repeated washes in phosphate buffer. Cells were incubated in DMEM media, with no phenol red, supplemented with 10% FBS in glass bottom dishes (HBSt-5030, Willco Wells) for all injection experiments. To deliver MBs and MB-conjugates in living cells, aqueous samples containing 5 μM antisense luciferase MBs and 10 μM Alexa750-labeled dextran or equivalent concentrations of MB-NeutrAvidin conjugates in phosphate buffer were microinjected into the cells. Following injection of the probe, fluorescent images were acquired every 5 min for a total of 60 min using an Olympus IX81 motorized inverted fluorescence microscope, as described below.

Microporation. Microporation was performed with an OneDrop MicroPorator (MP-100, BTX Harvard Apparatus) as per manufacturer's protocol. Specifically, MEF/3T3 cells were seeded in T-25 flasks in DMEM-FBS with no phenol red and no antibiotics 1 day prior to microporation. Before microporation, the cells were trypsinized, pelleted and resuspended in media without phenol red and antibiotics, pelleted again, washed with 1× PBS, and resuspended in resuspension buffer R (BTX Harvard Apparatus) at a concentration of 120 000 cells per 11 μl. To deliver MBs into the cells, 1 μl of sample containing MBs and Alexa750-labeled dextran were added to the cells such that the final MB concentration and Alexa750-labeled dextran were 5 μM and 10 μM, respectively. To deliver MB-NeutrAvidin conjugates into cells, 1 μl of NeutrAvidin-MB conjugates were added to the cells such that the final concentration of MBs was also 5 μM. Ten microliters of the cells (i.e. 100 000 cells) incubated in the presence of the probes were then microporated at 1500 V with a 10-ms pulse width and three pulses total. Following microporation the cells were wash once in 1× PBS and resuspended in the DMEM (without phenol red and supplemented with 10% FBS) and then seeded into the 8-well Lab-Tek Chambered Coverglass (155409, Nalge Nunc) or Glass bottom Dish (Willco Wells). Fluorescence images were acquired ~10 min (i.e. immediately after seeding cell seeding), 1, 2, 3, 4, 5 and 24 h after microporation.

Preparation of fluorescent water-in-oil emulsions

Water-in-oil emulsions were prepared as previously described (32). Briefly, Span 89 (447 mg) and Tween-80 (54 mg) were added to mineral oil (24 g) and the mixture was vortexed vigorously. A 3-ml aliquot of this sample was then added to a glass vial and stirred. An aqueous sample containing either 5-μM MBs and 10-μM Alexa-750-labeled dextran or 5-μM MB-NeutrAvidin conjugates was then added dropwise to form a microemulsion. An aliquot of the emulsion sample was placed on a coverslip for microscopic analysis.

Fluorescent microscopy

All microscopy images were performed on an Olympus IX 81 motorized inverted fluorescence microscope equipped with a back-illuminated EMCCD camera. (Andor), an X-cite 120 excitation source (EXFO) and Sutter excitation and emission filter wheels. Images of TEX615 Texas Red and Alexa750 were acquired using the filter sets (HQ560/55, HQ645/75, Q595LP) and (HQ710/75, HQ810/90, Q750LP) (Chroma), respectively, with short exposure times to avoid unnecessary photobleaching of the dyes. A LUC PLAN FLN 40× objective (NA 0.9) was used for all imaging studies. Results were analyzed with NIH Image J.

Ratiometric analysis

Water-in-oil emulsions. Emulsions containing MBs and fluorescently labeled dextrans or MB-NeutrAvidin conjugates were prepared as described above. For each water-in-oil bubble, two images were acquired, one corresponding to the Molecular Beacon reporter dye (i.e. Texas Red) and the other to the reference dye (i.e. Alexa750) on the dextran or NeutrAvidin. A region of interest (ROI) was drawn around each bubble, and the total fluorescent intensity was measured in each image. Similarly, the total fluorescence intensity from an equal size ROI drawn around a background region was also measured for each image. The background subtracted fluorescence measurement for the MB and the reference moiety was then calculated. The fluorescence ratio, F_{MB}/F_{ref}, was then calculated by dividing the background subtracted MB fluorescence by the background subtracted reference fluorescence.

Ratiometric analysis was performed on images of MEF/3T3 cells using a method analogous to that used for water-in-oil emulsions, with an additional step to subtract autofluorescence from the cells. For these studies, the ROI was drawn around individual cells. For microinjection, autofluorescence was determined by acquiring images of the cell in the channels corresponding to the MB and reference signals, respectively, prior to microinjection. For microporation, the average cellular autofluorescence was determined at various time points following microporation of cells without any probes. At least 10 cells were analyzed for each experiment.

Analysis of MB nonspecific interactions/degradation

When MBs are introduced into living cells, they often emit a false-positive signal as a result of nonspecific interactions and/or nuclease degradation. To determine the extent of this nonspecific opening, the fluorescence ratio, F_{MB}/F_{ref}, was first determined for individual cells and microemulsion samples as described above. Then, the percent of MBs opened could be calculated as the follows:

$$\%\ MBs\ opened = \frac{R_{CELL} - R_{BUBBLES,CLOSED}}{R_{BUBBLES,OPENED} - R_{BUBBLES,CLOSED}} \quad \mathbf{1}$$

where R_{CELL} is the fluorescence ratio, F_{MB}/F_{ref}, in living cells, and $R_{BUBBLES,\ MB\ CLOSED}$ and $R_{BUBBLES,\ OPENED}$

refer to the fluorescent ratio, F_{MB}/F_{ref}, for the unhybridized and fully hybridized MBs in aqueous bubbles prepared from water-in-oil emulsions, respectively.

Functionality assay

Aqueous samples containing 100-μM synthetic nucleic acid targets complementary to the MBs in 1× PBS, pH 7.4 were microinjected into MEF/3T3 cells containing MBs or MB-conjugates. The targets were injected into cells at 3–5 h and 24 h post-microporation. Fluorescent images of each cell were acquired immediately before and shortly after injection.

RESULTS AND DISCUSSION

Subcellular trafficking and nonspecific opening of MBs and MB-NeutrAvidin conjugates following microinjection

Previously, we have shown that when nonsense DNA- and 2Me MBs are introduced into living cells by microinjection they are quickly sequestered into the nucleus and emit a false-positive signal (12,13). Here we evaluated whether MBs having stem and loop domains composed of both 2Me RNA bases and phosphorothioate internucleotide linkages (2MePS) emit similar false-positive signals. Results were compared with an analogous MB composed purely of a 2Me RNA backbone. Since PS linkages have previously been shown to be highly resistant to nuclease digestion (29,33), it was hypothesized that if the nonsense 2MePS MBs exhibited any increase in fluorescence it would likely reflect nonspecific protein interactions. It should be noted that although 2Me oligonucleotides are also known to exhibit improved nuclease resistance compared with DNA, it has been shown that they are still susceptible to intracellular nuclease degradation (34–37).

2Me MBs. In agreement with our previous findings (13), immediately following the cytoplasmic injection of nonsense 2Me MBs into MEF-3T3 cells, the majority of the 2Me MBs were sequestered into the nucleus, where they seemed to emit a bright fluorescent signal (Figure 1A). To determine whether the apparent increase in fluorescence was simply due to the accumulation of MBs in the nucleus or the emission of a false-positive signal, the percentage of MBs that were open was quantified as a function of time. This was accomplished through the simultaneous injection of reference dyes (Alexa750-labeled dextran) and 2Me MBs and the subsequent determination of the fluorescent ratio (i.e. total integrated MB fluorescence/total integrated Alexa750 fluorescence, F_{MB}/F_{ref}). An important benefit of performing a ratiometric analysis is that it allows for normalization against cell-to-cell variations in MB fluorescence that

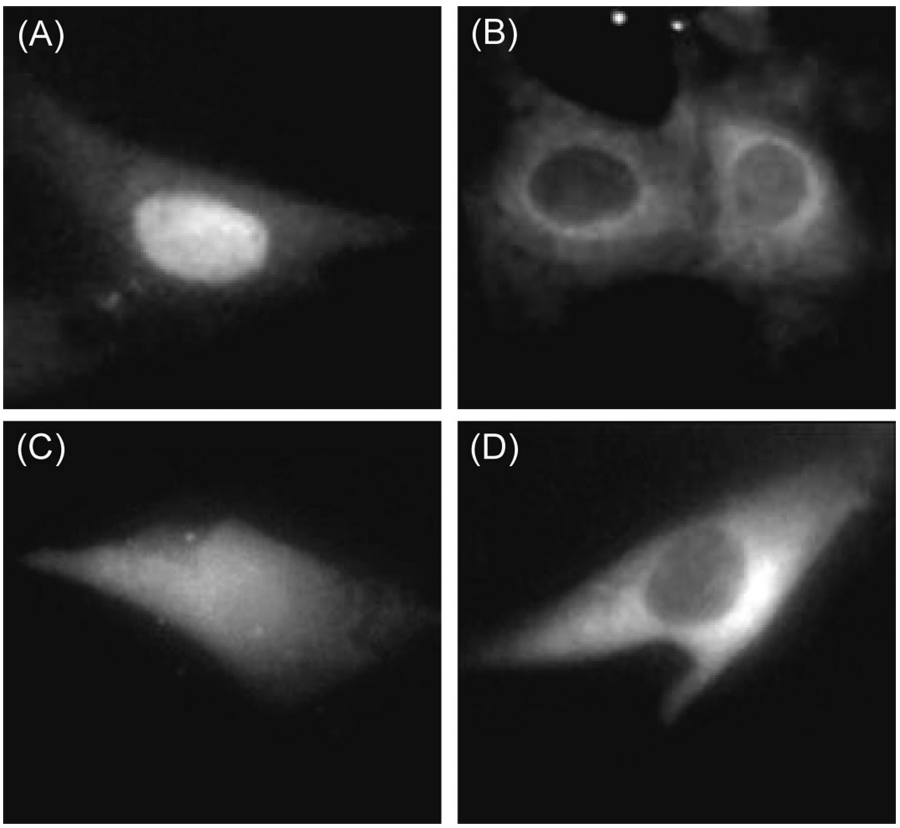

Figure 1. Fluorescence images of MBs and MB-NeutrAvidin conjugates following microinjection in living MEF/3T3 cells. The representative images shown were acquired 20 min following the injection of (**A**) 2Me MBs, (**B**) 2Me MB-NeutrAvidin conjugates, (**C**) 2MePS MBs and (**D**), 2MePS MB-NeutrAvidin conjugates. The MBs used were not complementary to any known endogenous RNA in MEF/3T3 cells.

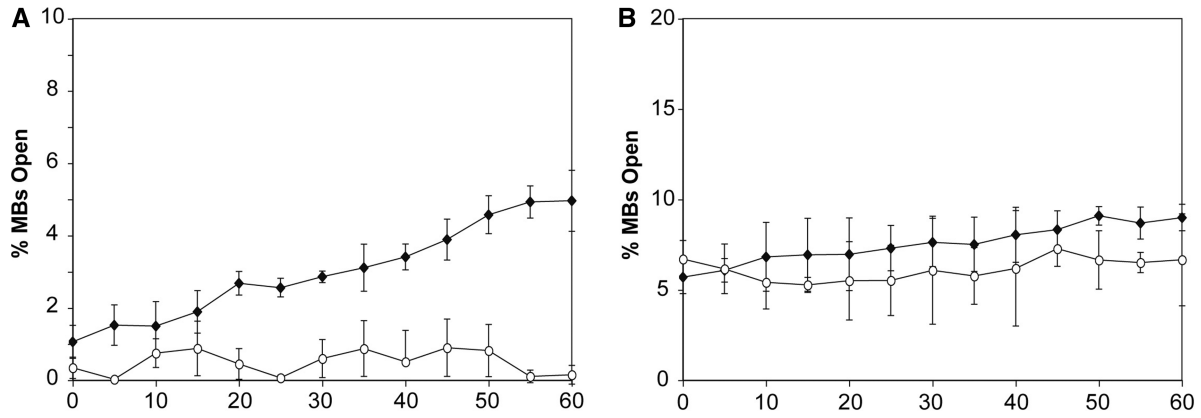

Figure 2. Temporal measurements of nonspecific MB opening, following microinjection into MEF/3T3 cells. Nonsense (**A**) 2Me MBs (filled diamonds) and 2Me MB-NeutrAvidin conjugates (open circles) as well as (**B**) 2MePS MBs (filled diamonds) and 2MePS MB-NeutrAvidin conjugates (open circles) were microinjected into living cells and fluorescence images were acquired every 5 min for 60 min. Quantification of MB opening was calculated as described in the 'Materials and methods' section. Each data point represents that mean and standard deviation from three to four cells.

result from differences in the efficiency of probe delivery. To quantify the percent of MBs that were open, the intracellular ratio was compared with fluorescence microscopy measurements of the same MB-dextran samples prior to intracellular delivery (Supplementary Figure S1). Specifically, water-in-oil emulsions were prepared with the MB-dextran samples in the absence and presence of target, representing 0% and 100% opening of the MBs, respectively. Images of the fluorescent bubbles were then acquired directly on the microscope and the ratio, F_{MB}/F_{ref}, was calculated. Using these extracellular measurements as standards, the percent of open MBs within living cells could readily be determined. It should be noted that this assumes that each MB is either in an open or closed state, with no intermediate levels of fluorescence. This is unlikely, but was done for simplification.

It was found that following the intracellular delivery of 2Me MBs, the percent of MBs that were open increased from 1.06% ± 0.45% (SE) to 5% ± 0.84% (SE) over the course of 60 min (Figure 2A). In order to confirm that the increase in fluorescence was not due to undesirable MB hybridization or sequence-specific protein interactions, live cell competitive inhibition studies were performed. Specifically, an excess of linear 2Me RNAs, with the same targeting sequence as the MBs, were co-injected with MBs into the MEF-3T3 cells. It was expected that if the MB signal were do to target hybridization or sequence-specific protein interactions, then the 2Me RNAs would compete for the same binding sites and reduce/eliminate the fluorescent signal. Despite injections of 10-fold molar excess of 2Me RNAs, we still observed an increase in cellular fluorescence. These findings suggest that the false-positive signals likely result from nuclease degradation and/or nonspecific protein interactions.

2Me MB-NeutrAvidin conjugates. When 2Me MBs were conjugated to fluorescently-labeled, pegylated NeutrAvidin prior to injection into MEF-3T3 cells, fluorescent signals from the MBs were predominantly observed within the cytoplasm over the course of 60 min (Figure 1B). On average only 0.34% ± 0.30% were opened by nonspecific interactions in living cells immediately following cytoplasmic injection (Figure 2A), which was not significantly different from no opening ($P = 0.12$, two-tailed t-test assuming equal variance). Further, no statistically significant increase in fluorescence was observed for at least 60 min. These results are similar to those previously observed with DNA MB-Quantum dot conjugates and suggest that MBs remain intact and in a quenched hairpin conformation when limited to the cytoplasmic compartment (12).

2MePS MBs. When 2MePS MBs were injected into the cytoplasm of living cells, they exhibited behavior that was distinct from the analogous 2Me MBs. Specifically, the 2MePS MBs exhibited much slower nuclear trafficking, with little nuclear localization evident even 20 min after microinjection (Figure 1C). However, by 1 h the 2MePS MBs were also found to reside predominantly in the nucleus. In addition to the slower nuclear trafficking, it was also found that a fraction [5.7 ± 0.91% (SE)] of 2MePS MBs opened immediately following injection into MEF3T3 cells. This immediate increase in fluorescence was not observed with 2Me MBs. Little further increase in 2MePS MB fluorescence was observed over the next 60 min (Figure 2B). Competitive inhibition experiments, with linear 2MePS RNAs that target the same sequence as the MBs, were used to confirm that the false-positive signal was not the result of RNA hybridization or sequence-dependent protein interactions.

2MePS MB-NeutrAvidin conjugates. When 2MePS MBs were coupled to NuetrAvidin prior to injection into living cells, as expected, MB fluorescence was only observed in the cytoplasm (Figure 1D); however, there was still an immediate increase in the fluorescent ratio, F_{MB}/F_{ref}, which corresponded to 6.70 ± 1.02% of the MBs being open. There was no further increase in MB opening over the next 60 min (Figure 2B). In general, the addition of

NeutrAvidin did not result in any statistically significant improvement in the prevention of false-positive signals, as it did with 2Me MBs.

Long-term subcellular trafficking, nonspecific opening and functionality of MBs and MB-NeutrAvidin conjugates

Although microinjection can be used to deliver MBs and MB-NeutrAvidin conjugates directly into the cytosol of living cells, this method is tedious, inefficient and impractical for the long-term analysis of gene expression in large numbers of cells. Recently, we found that microporation offers an efficient alternative (www.microporator.com) (13). Microporation is a microliter-volume electroporation process that exhibits a reduction in the many harmful events often associated with electroporation, including heat generation, metal ion dissolution, pH variation and oxide formation. When used to deliver MB-NeutrAvidin conjugates into MEF-3T3 cell, microporation exhibited a transfection efficiency of >93% (i.e. percent of cells with probes inside) and an average cell viability of 86% (13). Therefore, microporation was adopted here as a delivery method to facilitate the long-term analysis of 2Me and 2MePS MBs, as well as the corresponding MB-NeutrAvidin conjugates in living cells.

2Me MBs. When nonsense 2Me MBs were microporated into MEF-3T3 cells, they were immediately sequestered into the nucleus (<10 min) with only a small fraction remaining in the cytoplasm (Figure 3A). This was similar to what was observed following microinjection. No significant change in the intracellular distribution was observed over the next 5 h; however, by 24 h after microporation many bright fluorescent spots could be observed in the cytoplasm. Co-localization of these bright spots with the lysosomal labeling dye, LysoTracker, indicated that these MBs were entrapped within lysosomes. Nonetheless, a significant number of MBs could still be observed in the nucleus.

Quantification of the fluorescent images revealed that ~15% of the 2Me MBs were opened nonspecifically within 10 min after microporation (Figure 4A). This was significantly higher that what was observed at a similar time after microinjection, where only ~2% of the MBs were open. It is hypothesized that this increase in nonspecific opening may reflect an increase in nuclease activity following microporation. After the initial jump in nonspecific opening, the percent of open MBs steadily increased to ~50% over the next 24 h. Although it can be argued that the increase in false-positive signals reflects the degradation of MBs in lysosomes, it appears that a significant degree of false-positive signals are observed even prior to any significant lysosomal entrapment was observed.

To determine whether 2Me MBs were still functionally active at various times after microporation, complementary RNA targets were injected into individual cells 3 h and 24 h after microporation (Figure 5A). Fluorescent measurements were then acquired to determine whether any increase in fluorescence, corresponding to MB hybridization, could be detected. After 3 h, functional MBs were observed in both the cytoplasm and the nucleus. Conversely, after 24 h no enhancement in fluorescence was observed after injection of the nucleic acid targets. This was quite surprising considering that a relatively diffuse fluorescent signal could be observed in the nucleus of most cells (and to a lesser extent the cytoplasm), giving the appearance that these MBs were available for hybridization, but in fact they were not.

Based on the above findings, there appear to be several lines of evidence that suggest nuclease degradation is responsible for the false-positive MB signals. For example, there is a significant disparity between the rate of nuclear sequestration and the rate of false-positive signal generation. It is expected that there would be a better correlation between these two events if nonspecific interactions in the nucleus were the cause of the false-positive signal. Further, it seems unlikely that nonspecific interactions would only occur in the nucleus and not the cytoplasm, which is what was observed. The continual increase in false-positive signals over time also seems to better match what would be expected for enzymatic degradation. Finally, 24 h after microporation a diffuse fluorescent signal could still be observed in the cytoplasm and nucleus, but none of these MBs was functional. This seems consistent with the presence of degraded MB side-products.

2Me MB-NeutrAvidin conjugates. When 2Me MB-NeutrAvidin conjugates were microporated into MEF-3T3 cells, they localized primarily in the cytoplasm of the cell although a faint fluorescent signal could also be observed in the nucleus (Figure 3A). Within several hours, it became clear that some MB-NeutrAvidin conjugates had indeed passed through the nuclear pores. This was not observed following microinjection. Presumably, the passage of MB-NeutrAvidin conjugates into the nucleus arose from the transient permeablization of the nuclear membrane during microporation. Within 5 h, the majority of the 2Me MB-NeutrAvidin conjugates were determined to be in lysosomes. Only a faint fluorescent signal remained in the cytosol and nucleus at this time point. This seems to indicate that the attachment of NeutrAvidin to MBs encourages nonspecific interactions, even when heavily pegylated. By 24 h, the majority of the MBs seemed to be localized within lysosomes.

Taking into consideration the gradual trafficking of MB-NeutrAvidin conjugates to lysosomes following microporation, it was not surprising to find that there was also an increase in the nonspecific opening of MBs. Quantitative analysis of these fluorescent signals indicated that the percent of MBs opened over the course of 4 h increased from 4% to 20%, but then plateaued (Figure 4A). No further increase in MB fluorescence was observed even at 24 h. Interestingly, this may indicate that the false-positive signal arose from nuclear localization, not lysosomal localization, since there was clearly an increase in lysosomal entrapment between 5 and 24 h. Conversely, there was no clear increase in nuclear localization after the initial permeabilization of the nuclear

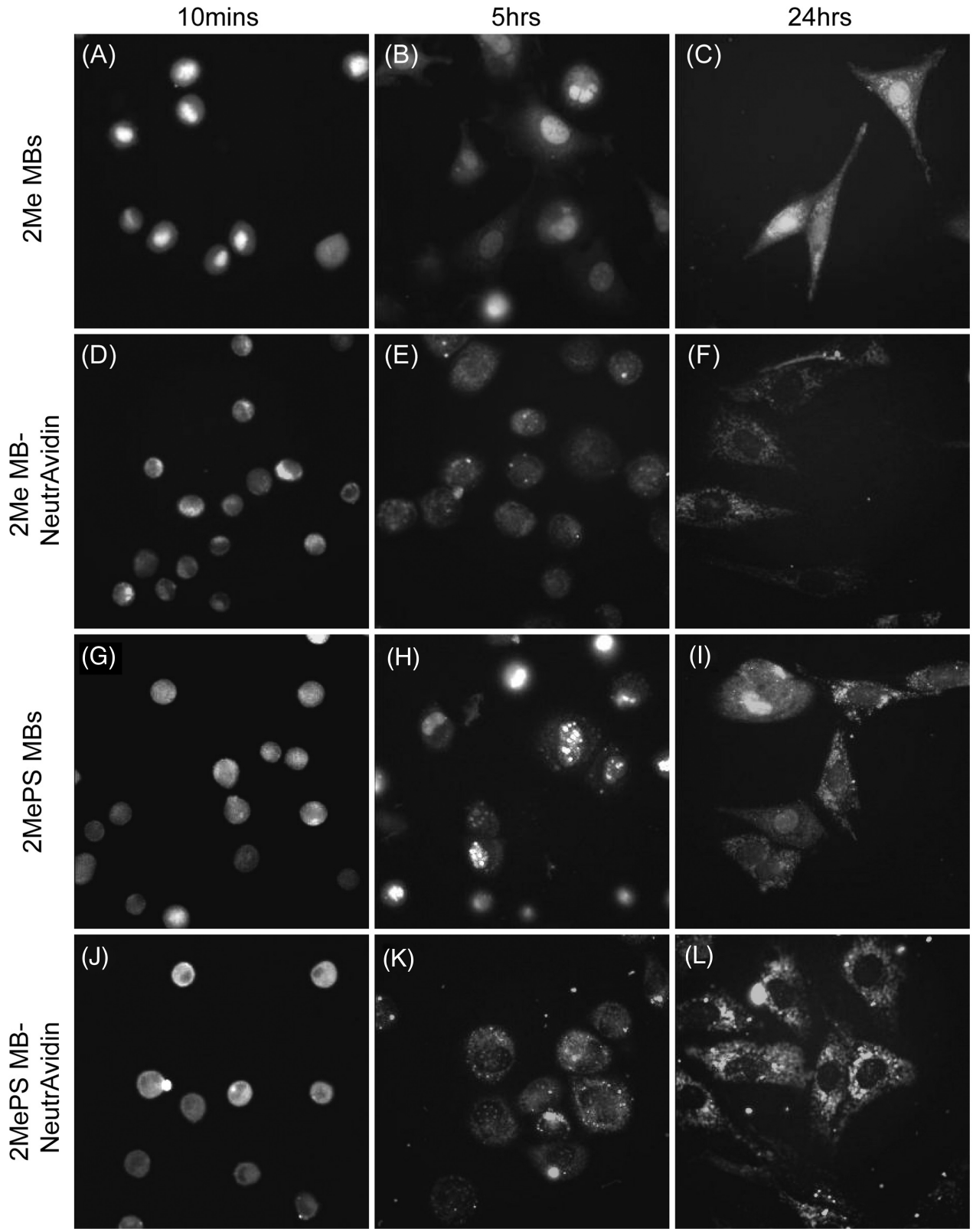

Figure 3. Fluorescence images of MBs and MB-NeutrAvidin conjugates in living MEF/3T3 cells at various time points after microporation. Images of the MB signals are shown for 2Me MBs at (**A**) 10 min, (**B**) 5 h and (**C**) 24 h and for 2Me MB-NeutrAvidin conjugates at (**D**) 10 min, (**E**) 5 h and (**F**) 24 h following microporation. Likewise, images of the 2MePS MBs acquired at (**G**) 10 min, (**H**), 5 h, (**I**) 24 h and images of the 2MePS MB-NeutrAvidin conjugates acquired at (**J**) 10 min, (**K**) 5 h, (**L**) or 24 h after microporation in MEF/3T3 cells are also shown.

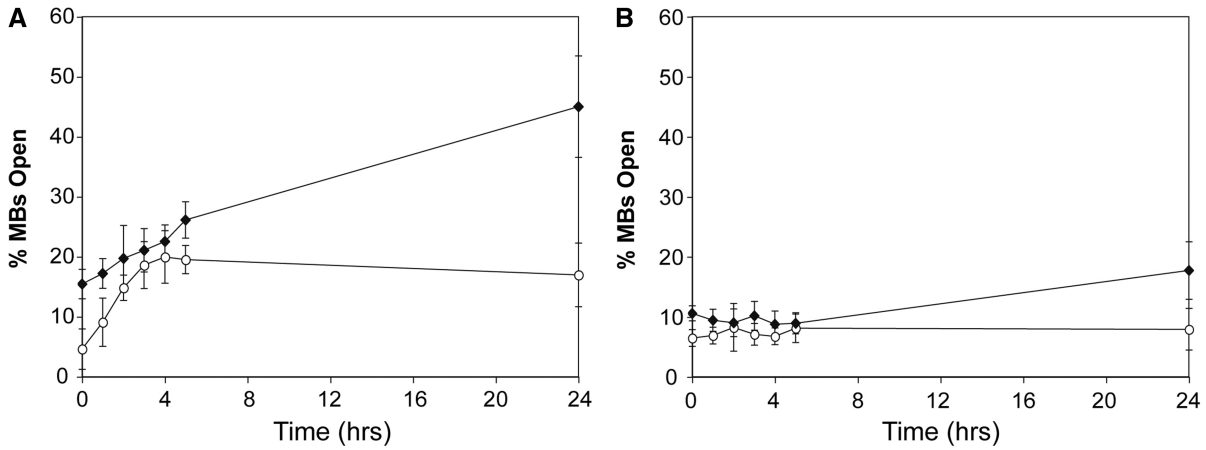

Figure 4. Temporal measurements of non-specific MB opening, following microporation into MEF/3T3 cells. Nonsense (**A**) 2Me MBs (filled diamonds) and 2Me MB-NeutrAvidin conjugates (open circles) as well as (**B**) 2MePS MBs (filled diamonds) and 2MePS MB-NeutrAvidin conjugates (open circles) were microporated into living cells and fluorescence images were acquired over the course of 24 h. Quantification of MB opening was calculated as described in the 'Materials and Methods' section. Each data point represents that mean and standard deviation from at least 10 cells.

membrane, likely because the NeutrAvidin prevented further entry.

Although 2Me MBs and 2Me MB-NeutrAvidin conjugates were both found to emit false-positive signals, the presence of NeutrAvidin did seem to reduce the percent of MBs that were opened nonspecifically at each of the time points tested. Further, in contrast to 2Me MBs, there were still some 2Me MB-NeutrAvidin conjugates that remained functionally active after 24 h (Figure 5B). Specifically, when complementary nucleic acid targets were injected into the cytoplasm of cells, 24 h after being microporated with 2Me MB-NeutrAvidin conjugates, an increase in fluorescence was observed throughout the cytosol and nucleus. These observations suggest that a fraction of the 2Me MB-NeutrAvidin conjugates still resided in the cytosol and could still hybridize to target nucleic acids. If all of the 2Me MB-NeutrAvidin conjugates were entrapped within lysosomes, they likely would not have had access to the complementary nucleic acids that were injected. Therefore, it appears the incorporation of NeutrAvidin into the MB design also added some benefit on the long-term functionality of the MBs.

2MePS MBs. When 2MePS MBs were delivered into MEF-3T3 cells via microporation, they initially appeared to be distributed uniformly throughout the cell; however, over time it did become evident that they were being trafficked to the nucleus (Figure 3B). The rate at which 2MePS MBs were trafficked to the nucleus was clearly far slower than the analogous 2Me MBs, taking hours as opposed to minutes. Interestingly, the 2MePS MBs that were observed in the nucleus seemed to localize primarily within the nucleoli (Figure 4B). By 5 h after microporation, the majority of the 2MePS MB actually resided in the nucleoli, although some evidence of lysosomal entrapment also became apparent. By 24 h the 2MePS MBs were found primarily in lysosomes, with only a faint fluorescent signal remaining in the cytosol and nucleus.

Quantification of the fluorescent images revealed that ~10% of the 2MePS MBs were opened immediately following microporation; however, no further increase in fluorescence was observed over the next 5 h and only a slight increase in fluorescence was observed after 24 h (Figure 4B). The initial jump in 2MePS MB fluorescence is quite distinct from the slow increase in fluorescence observed with 2Me MBs. These differences may reflect alternative mechanisms by which the false-positive signals are generated. It is hypothesized that the 2MePS MBs are more susceptible to nonspecific protein interactions, whereas the 2Me MBs are more susceptible to nuclease degradation. A higher extent of non-specific interactions may explain why 2MePS MBs exhibited higher levels of lysosomal entrapment compared with the 2Me MBs. Interestingly, despite the high degree of lysosomal entrapment, it was found that some 2MePS MBs did still reside in the cytoplasm and these MBs were still functionally active, i.e. they were still capable of hybridizing complementary nucleic acid targets, 3 h and 24 h after microporation, respectively (Figure 5C).

2MePS MB-NeutrAvidin conjugates. When 2MePS MBs were conjugated to NeutrAvidin, they were found to behave very similar to the 2Me MB-NeutrAvidin conjugates, following microporation into MEF-3T3 cells. Specifically, although initially they appeared to be relatively diffused in the cytoplasm, within several hours the majority of the 2MePS MB-NeutrAvidin conjugates were found in lysosomes (Figure 3B). Moreover, it appeared that the microporation procedure also allowed some of the 2MePS MB-NeutrAvidin conjugates to pass through the nuclear pores, as some fluorescent signal were observed in the nucleus. By 24 h, nearly all of the 2MePS MB-NeutrAvidin conjugates were localized within lysosomes.

While the distribution and trafficking of the 2MePS MB-NeutrAvidin conjugates mirrored that of the 2Me MB conjugates, the fluorescent emission was actually quite different. Specifically, the 2MePS MBs exhibited an

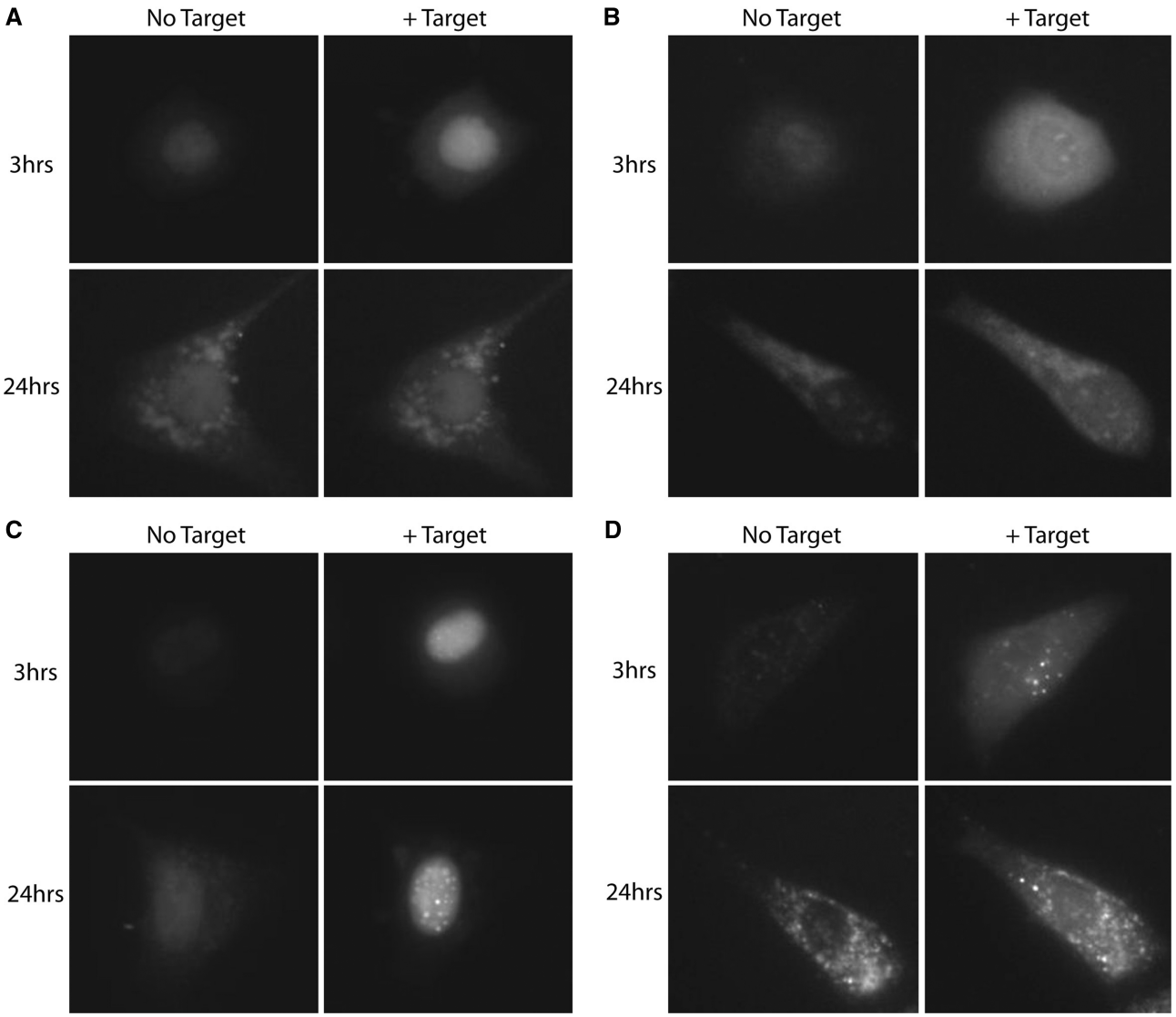

Figure 5. Evaluation of MB functionality in MEF/3T3 cells at various times after microporation. Excess complementary nucleic acid targets were injected into MEF/3T3 cells 3 h and 24 h after being microporated with (**A**) 2Me MBs, (**B**) 2Me MB-NeutrAvidin conjugates, (**C**) 2MePS MBs and (**D**) 2MePS MB-NeutrAvidin conjugates. Fluorescent images of the cells were acquired immediately before and shortly after microinjection. Representative fluorescent images are shown.

immediate increase in fluorescence corresponding to ~8% of the MBs being opened nonspecifically, but then no further increase in fluorescence was observed over the next 24 h (Figure 4B). This is in sharp contrast to the time-dependent increase in fluorescence observed with the 2Me MB-NeutrAvidin conjugates and more closely resembles the behavior of the unconjugated 2MePS MBs. These findings seem to further support our hypothesis that phosphorothioate linkages are resistant to nuclease degradation, but are more susceptible to nonspecific protein interactions.

Overall, the attachment of NeutrAvidin to 2MePS MBs did reduce their nuclear sequestration, as expected; however, it also led to the accelerated trafficking of the MBs to lysosomes and only provided a marginal reduction in the false-positive signal. Therefore, the presence of NeutrAvidin did not seem to yield the same advantages as it did with 2Me MBs.

To evaluate whether the 2MePS MB-NeutrAvidin conjugates were still functional 3 h and 24 h following microporation, complementary nucleic acid targets were microinjected into single cells at these two time points (Figure 5D). As expected, at least some MBs were still functional at both times.

CONCLUSION

Although numerous studies have shown that MBs can be used to visualize endogenous RNA in living cells, the susceptibility of MBs to nonspecific interactions and/or nuclease degradation and the resulting false-positive signals has limited their use to the study of highly

overexpressed RNA. This has led to the evaluation of alternative nucleic acid chemistries that are intended to confer increased resistance to nuclease degradation and less susceptibility to nonspecific interactions. In this study, we systematically analyzed the subcellular trafficking, false-positive signal generation, and functionality of MBs with 2Me and 2MePS modifications. Interestingly, it was found that 2Me MBs, which are perhaps the most widely utilized MB composition, were highly susceptible to nonspecific interactions and/or nuclease degradation and emitted a false-positive signal that increased with time. These false-positive signals, however, could be completely eliminated simply by attaching the MBs to NeutrAvidin, which prevented their translocation to the nucleus; at least when microinjection was used to deliver the MB-NeutrAvidin conjugates into living cells. Unfortunately, the absence of false-positive signals did not carryover to when microporation was used to deliver the MB-NeutrAvidin conjugates. In addition, false-positive signals could not be eliminated when 2MePS MBs were utilized regardless of whether or not they were conjugated to NeutrAvidin. Therefore, if highly sensitive measurements of RNA expression are required, 2Me MB-NeutrAvidin conjugates seem to provide the best option. This was the only strategy tested that did not result in any detectable false-positive signals. Of course, one concern with incorporating NeutrAvidin into the MB design is that it could impede the free diffusion of the MBs in the cytoplasm, thereby reducing hybridization kinetics. Alternatively, NeutrAvidin could potentially reduce the accessibility of MBs to any RNAs associated with cytosolic proteins. These possible shortcomings must be taken into consideration when using MB-NeutrAvidin conjugates.

When a more high-throughput approach to studying gene expression is required, then 2Me MB-NeutrAvidin conjugates no longer provide a suitable option for highly sensitive measurements of RNA due to the high level of nonspecific MB opening observed following microporation. Even more problematic was that the extent of false-positives increased with time. The 2MePS MBs also opened nonspecifically following microporation, but to a much lower extent and the false-positive signal did not vary with time, making it easier to account for. NeutrAvidin could also be conjugated to 2MePS MBs to reduce nuclear sequestration, although the addition of NeutrAvidin did not seem to result in any significant improvement in reducing the false-positives.

It should be noted that although the results that were presented here were for MEF-3T3 cells, similar findings were also obtained with HeLa and MCF-7 cells (data not shown). Therefore, we believe the behavior observed is true in general and not specific for MEF-3T3 cells.

Overall, these results suggest that the optimal MB backbone may be dependent on the mechanism of delivery. Further, we demonstrate that oligonucleotide modifications can have a profound impact on the fate of MBs in the intracellular environment, highlighting the need to continue evaluating alternative MB designs.

SUPPLEMENTARY DATA

Supplementary Data are available at NAR Online.

FUNDING

The National Institutes of Health (National Cancer Institute) R21 CA116102 and R21-CA125088; the National Science Foundation BES-0616031; and the American Cancer Society RSG-07-005-01. Funding for open access charge: The National Institutes of Health (National Cancer Institute) R21 CA116102 and R21-CA125088; the National Science Foundation BES-0616031; and the American Cancer Society RSG-07-005-01.

Conflict of interest statement. M.A.B. is employed by Integrated DNA Technologies, Inc., (IDT) which offers oligonucleotides for sale similar to some the compounds described in the manuscript. IDT is however not a publicly traded company and the author personally does not own any shares/equity in IDT.

REFERENCES

1. Elowitz,M.B., Levine,A.J., Siggia,E.D. and Swain,P.S. (2002) Stochastic gene expression in a single cell. *Science*, **297**, 1183–1186.
2. Gander,M.J., Mazza,C. and Rummler,H. (2007) Stochastic gene expression in switching environments. *J. Math. Biol*., **55**, 249–269.
3. Mettetal,J.T., Muzzey,D., Pedraza,J.M., Ozbudak,E.M. and van Oudenaarden,A. (2006) Predicting stochastic gene expression dynamics in single cells. *Proc. Natl Acad. Sci. USA*, **103**, 7304–7309.
4. Raj,A. and van Oudenaarden,A. (2008) Nature, nurture, or chance: stochastic gene expression and its consequences. *Cell*, **135**, 216–226.
5. Thattai,M. and van Oudenaarden,A. (2004) Stochastic gene expression in fluctuating environments. *Genetics*, **167**, 523–530.
6. Levsky,J.M., Shenoy,S.M., Pezo,R.C. and Singer,R.H. (2002) Single-cell gene expression profiling. *Science*, **297**, 836–840.
7. Lu,J. and Tsourkas,A. (2009) Imaging individual microRNAs in single mammalian cells in situ. *Nucleic Acids Res*., **37**, e100.
8. Raj,A., Peskin,C.S., Tranchina,D., Vargas,D.Y. and Tyagi,S. (2006) Stochastic mRNA synthesis in mammalian cells. *PLoS Biol*., **4**, e309.
9. Raj,A., van den Bogaard,P., Rifkin,S.A., van Oudenaarden,A. and Tyagi,S. (2008) Imaging individual mRNA molecules using multiple singly labeled probes. *Nat. Methods*, **5**, 877–879.
10. Tyagi,S. and Kramer,F.R. (1996) Molecular beacons: probes that fluoresce upon hybridization. *Nat. Biotechnol*., **14**, 303–308.
11. Bratu,D.P., Cha,B.J., Mhlanga,M.M., Kramer,F.R. and Tyagi,S. (2003) Visualizing the distribution and transport of mRNAs in living cells. *Proc. Natl Acad. Sci. USA*, **100**, 13308–13313.
12. Chen,A.K., Behlke,M.A. and Tsourkas,A. (2007) Avoiding false-positive signals with nuclease-vulnerable molecular beacons in single living cells. *Nucleic Acids Res*., **35**, e105.
13. Chen,A.K., Behlke,M.A. and Tsourkas,A. (2008) Efficient cytosolic delivery of molecular beacon conjugates and flow cytometric analysis of target RNA. *Nucleic Acids Res*., **36**, e69.
14. Drake,T.J., Medley,C.D., Sen,A., Rogers,R.J. and Tan,W. (2005) Stochasticity of manganese superoxide dismutase mRNA expression in breast carcinoma cells by molecular beacon imaging. *Chembiochem*, **6**, 2041–2047.
15. Mhlanga,M.M., Vargas,D.Y., Fung,C.W., Kramer,F.R. and Tyagi,S. (2005) tRNA-linked molecular beacons for imaging mRNAs in the cytoplasm of living cells. *Nucleic Acids Res*., **33**, 1902–1912.
16. Nitin,N. and Bao,G. (2008) NLS peptide conjugated molecular beacons for visualizing nuclear RNA in living cells. *Bioconjug. Chem*., **19**, 2205–2211.

17. Nitin,N., Santangelo,P.J., Kim,G., Nie,S. and Bao,G. (2004) Peptide-linked molecular beacons for efficient delivery and rapid mRNA detection in living cells. *Nucleic Acids Res.*, **32**, e58.
18. Peng,X.H., Cao,Z.H., Xia,J.T., Carlson,G.W., Lewis,M.M., Wood,W.C. and Yang,L. (2005) Real-time detection of gene expression in cancer cells using molecular beacon imaging: new strategies for cancer research. *Cancer Res.*, **65**, 1909–1917.
19. Perlette,J. and Tan,W. (2001) Real-time monitoring of intracellular mRNA hybridization inside single living cells. *Anal. Chem.*, **73**, 5544–5550.
20. Rhee,W.J. and Bao,G. (2009) Simultaneous detection of mRNA and protein stem cell markers in live cells. *BMC Biotechnol.*, **9**, 30.
21. Rhee,W.J., Santangelo,P.J., Jo,H. and Bao,G. (2008) Target accessibility and signal specificity in live-cell detection of BMP-4 mRNA using molecular beacons. *Nucleic Acids Res.*, **36**, e30.
22. Rodriguez,A.J., Condeelis,J., Singer,R.H. and Dictenberg,J.B. (2007) Imaging mRNA movement from transcription sites to translation sites. *Semin. Cell Dev. Biol.*, **18**, 202–208.
23. Santangelo,P., Nitin,N., LaConte,L., Woolums,A. and Bao,G. (2006) Live-cell characterization and analysis of a clinical isolate of bovine respiratory syncytial virus, using molecular beacons. *J. Virol.*, **80**, 682–688.
24. Santangelo,P.J., Nix,B., Tsourkas,A. and Bao,G. (2004) Dual FRET molecular beacons for mRNA detection in living cells. *Nucleic Acids Res.*, **32**, e57.
25. Tyagi,S. and Alsmadi,O. (2004) Imaging native beta-actin mRNA in motile fibroblasts. *Biophys. J.*, **87**, 4153–4162.
26. Vargas,D.Y., Raj,A., Marras,S.A., Kramer,F.R. and Tyagi,S. (2005) Mechanism of mRNA transport in the nucleus. *Proc. Natl Acad. Sci. USA*, **102**, 17008–17013.
27. Wang,W., Cui,Z.Q., Han,H., Zhang,Z.P., Wei,H.P., Zhou,Y.F., Chen,Z. and Zhang,X.E. (2008) Imaging and characterizing influenza A virus mRNA transport in living cells. *Nucleic Acids Res.*, **36**, 4913–4928.
28. Wu,Y., Yang,C.J., Moroz,L.L. and Tan,W. (2008) Nucleic acid beacons for long-term real-time intracellular monitoring. *Anal. Chem.*, **80**, 3025–3028.
29. Yeh,H.Y., Yates,M.V., Mulchandani,A. and Chen,W. (2008) Visualizing the dynamics of viral replication in living cells via Tat peptide delivery of nuclease-resistant molecular beacons. *Proc. Natl Acad. Sci. USA*, **105**, 17522–17525.
30. Dirks,R.W., Molenaar,C. and Tanke,H.J. (2001) Methods for visualizing RNA processing and transport pathways in living cells. *Histochem. Cell Biol.*, **115**, 3–11.
31. Li,J.J., Geyer,R. and Tan,W. (2000) Using molecular beacons as a sensitive fluorescence assay for enzymatic cleavage of single-stranded DNA. *Nucleic Acids Res.*, **28**, E52.
32. Chen,A.K., Cheng,Z., Behlke,M.A. and Tsourkas,A. (2008) Assessing the sensitivity of commercially available fluorophores to the intracellular environment. *Anal. Chem.*, **80**, 7437–7444.
33. Yoo,B.H., Bochkareva,E., Bochkarev,A., Mou,T.C. and Gray,D.M. (2004) 2′-O-methyl-modified phosphorothioate antisense oligonucleotides have reduced non-specific effects in vitro. *Nucleic Acids Res.*, **32**, 2008–2016.
34. Hoke,G.D., Draper,K., Freier,S.M., Gonzalez,C., Driver,V.B., Zounes,M.C. and Ecker,D.J. (1991) Effects of phosphorothioate capping on antisense oligonucleotide stability, hybridization and antiviral efficacy versus herpes simplex virus infection. *Nucleic Acids Res.*, **19**, 5743–5748.
35. Iribarren,A.M., Sproat,B.S., Neuner,P., Sulston,I., Ryder,U. and Lamond,A.I. (1990) 2′-O-alkyl oligoribonucleotides as antisense probes. *Proc. Natl Acad. Sci. USA*, **87**, 7747–7751.
36. Morvan,F., Porumb,H., Degols,G., Lefebvre,I., Pompon,A., Sproat,B.S., Rayner,B., Malvy,C., Lebleu,B. and Imbach,J.L. (1993) Comparative evaluation of seven oligonucleotide analogues as potential antisense agents. *J. Med. Chem.*, **36**, 280–287.
37. Summerton,J. and Weller,D. (1997) Morpholino antisense oligomers: design, preparation, and properties. *Antisense Nucleic Acid Drug Dev.*, **7**, 187–195.